Geomechanics and Engineering, *Vol. 38, No. 1 (2024) 93-106*
https://doi.org/10.12989/gae.2024.38.1.093

Probabilistic bearing capacity of circular footing on spatially variable undrained clay

Kouseya Choudhuri[a] and Debarghya Chakraborty*

Department of Civil Engineering, Indian Institute of Technology, Kharagpur-721302, India

(*Received December 20, 2022, Revised June 14, 2024, Accepted July 3, 2024*)

Abstract. The present paper investigates the spatial variability effect of soil property on the three-dimensional probabilistic characteristics of the bearing capacity factor (i.e., mean and coefficient of variation) of a circular footing resting on clayey soil where both mean and standard deviation of undrained shear strength increases with depth, keeping the coefficient of variation constant. The mean trend of undrained shear strength is defined by introducing the dimensionless strength gradient parameter. The finite difference method along with the random field and Monte Carlo simulation technique, is used to execute the numerical analyses. The lognormal distribution is chosen to generate random fields of the undrained shear strength. In the study, the potential failure of the structure is represented through the failure probability. The influences of different vertical scales of fluctuation, dimensionless strength gradient parameters, and coefficient of variation of undrained shear strength on the probabilistic characteristics of the bearing capacity factor and failure probability of the footing, along with the probability and cumulative density functions, are explored in this study. The variations of failure probability for different factors of safety corresponding to different parameters are also illustrated. The results are presented in non-dimensional form as they might be helpful to the practicing engineers dealing with this type of problem.

Keywords: circular footing; failure probability; Monte Carlo simulation; non-stationary random field; reliability index; spatial variability

1. Introduction

Consideration of the soil spatial variability has gained momentous importance over the past few decades. It incorporates the uncertainty associated with the soil parameters over space caused by variations in deposition and decomposition processes and loading or stress histories (Griffiths *et al.* 2002, Deng *et al.* 2021, 2022, Jiang *et al.* 2022). Three different types of spatial variability corresponding to a soil parameter were demonstrated by Lumb (1966) and Wu *et al.* (2019). Case I denotes the soil property having constant mean and standard deviation throughout the depth. Case II defines the soil property where the mean value linearly increases with depth, whereas the standard deviation remains independent of depth. Case III defines the soil property where both the mean and the standard deviation linearly increase with depth by keeping the *CoV* constant. Here, Case I is generally known as the stationary random field, whereas Case II and III are known as the non-stationary random fields. Several authors have studied different geomechanics problems considering stationary random fields (i.e., Case I). Such problems include the ultimate bearing capacity of shallow foundations (Griffiths *et al.* 2002, Al-Bittar and Soubra 2013, Jha 2016, Li *et al.* 2019, Krishnan and Chakraborty 2022, Das and Chakraborty 2024), foundation settlement (Fenton and Griffiths 2002, Griffiths and Fenton 2009), slope stability analyses (Griffiths and Fenton 2004, Cho 2010, Kasama and Whittle 2016, Lombardi *et al.* 2017, Bai *et al.* 2020), footing on reinforced slope (Halder and Chakraborty 2020a, Halder and Chakraborty 2020b), laterally loaded pile (Haldar and Sivakumar Babu 2008), pipe-soil system (Srivastava and Sivakumar Babu 2011), braced excavation (Luo *et al.* 2011), tunnel behaviour (Yoo 2016) and so forth. The spatial variability effect of cohesion on footing bearing capacity and slope stability was analyzed by Srivastava and Sivakumar Babu (2009), considering the Case II non-stationary random field. The Case II non-stationary random field for friction angle was also considered by Li *et al.* (2014) to check the reliability of an infinite slope. The Case III non-stationary random field is always restricted to the undrained shear strength (S_u) of clay as it is an effective stress-dependent parameter (Lumb 1966). Li *et al.* (2014) also checked the soil spatial variability effect on the reliability of infinite slope considering the Case III non-stationary random field for S_u. A similar type of non-stationary random fields was considered in different geotechnical structures such as strip footing (Li *et al.* 2015, Shen *et al.* 2019, 2021, Wu *et al.* 2019, 2020), skirted foundation (Charlton and Rouainia 2017), slope (Jamshidi Chenari and Alaie 2015, Zhu *et al.* 2017, Jiang and Huang 2018), and spudcan foundation (Shu *et al.* 2020, Yi *et al.* 2020).

The probabilistic analyses of three-dimensional shallow foundations (i.e., square, rectangular, circular, etc.) under

*Corresponding author, Ph.D.
E-mail: debarghya@civil.iitkgp.ac.in
[a]Ph.D. Student
E-mail: kousheyo1995@iitkgp.ac.in

ISSN: 2005-307X (Print), 2092-6219 (Online)

Table 1 (a) Domain effect and (b) mesh convergence study of the soil model considering $m = 0$

	Domain size of the soil model	Number of elements	N_c	% Difference
(a) Domain effect study	$6D \times 6D \times 2D$	6624	6.189	2.84
	$7D \times 7D \times 2.5D$	10920	6.126	1.795
	$8D \times 8D \times 3D$	16128	6.096	1.23
	$10D \times 10D \times 4D$	25344	6.018	-
(b) Mesh convergence study	$8D \times 8D \times 3D$	6048	6.667	10.217
		10500	6.323	4.53
		16128	6.096	0.711
		36480	6.049	-

random field framework are essential as they are constructed to carry heavy super-structural loads, and the potential risks associated with the failure of the system are needed to be appropriately assessed. Kawa and Pula (2020) explored the effect of soil spatial variability on the load carrying capacity of three-dimensional square and strip footings on cohesive-frictional soil. In the case of square footing, the probabilistic characteristics of load carrying capacity (μ_Q and CoV_Q) is found for different horizontal scales of fluctuation ($\theta_x = \theta_y$), whereas in the case of strip footing, the variations of μ_Q and CoV_Q are evaluated for different out-of-plane lengths of the model. It was observed that the two-dimensional analysis provides conservative results as compared to the three-dimensional analysis. Chawla and Kawa (2021) studied the three-dimensional probabilistic bearing capacity analysis of strip footing on a two-layer soil system considering the spatial variability effect of S_u of the bottom clay layer. In their study, the top layer is considered as a homogeneous (medium or dense) sand layer, and the bottom clay layer is modeled as the spatially varied non-stationary random field of S_u. The results were obtained for different strength gradient parameter, horizontal scale of fluctuation, and the top layer thickness under modified random failure mechanism method (RFMM) and compared with the random finite difference method (RFDM). Choudhuri and Chakraborty (2024) carried out a probability-based study on the bearing capacity responses of square and rectangular footings resting on spatially variable granular soil under rotated anisotropic framework. From the extensive literature survey, it is found that the three-dimensional analyses of circular footing considering the spatial variability of the soil properties are very limited. Choudhuri and Chakraborty (2022, 2023) studied the effect of spatial variability on the three-dimensional bearing capacity of a circular footing resting on a two-layer c-ϕ soil and single layer of granular soil, respectively. However, the non-stationary effect of the soil properties was not considered in their study. As far as the authors' knowledge, no study covers the probabilistic analysis of a three-dimensional circular footing considering the non-stationary random field of S_u. Hence, the present paper explores the soil spatial variability effect on a rough, rigid surface circular footing resting on clay following the Case III non-stationary random field under vertical loading.

The S_u at any arbitrary depth z below the ground surface can be expressed using the following equation (Bishop 1966)

$$S_u = S_{u0} + \frac{mzS_{u0}}{D} \tag{1}$$

where S_{u0} denotes the undrained shear strength at the ground surface, m is the dimensionless strength gradient parameter, and D represents the diameter of the footing. The four values of m (m = 0, 1, 2, 3) are being considered in this study. The results are presented in dimensionless bearing capacity factor (N_c) terms defined by

$$N_c = \frac{q_u}{S_{u0}} \tag{2}$$

where q_u denotes the ultimate bearing capacity of the footing.

The random finite-difference (RFDM) method under the Monte Carlo simulation (MCS) framework is incorporated to conduct the probabilistic analyses. Several methods have been utilized to simulate the random field, such as the local average subdivision (LAS) method (Griffiths *et al.* 2002), the covariance matrix decomposition method (Haldar and Sivakumar Babu 2008, Kasama and Whittle 2016, Choudhuri and Chakraborty 2022, 2023, 2024), K-L expansion method (Cho 2010, Krishnan and Chakraborty 2022, Li *et al.* 2022), Fourier series method (FSM) (Jha 2016, Kawa and Pula 2020), the spectral representation method (SRM) (Wu *et al.* 2019). With the advancement of computational facility, several advanced and efficient techniques have been developed in recent years, which are the Fast Fourier Transform-Moving Average (FFT-MA) (Li *et al.* 2021), conditional random field with maximum likelihood method and Markov Chain Monte Carlo (MCMC) method (Zhao *et al.* 2021). However, the present study uses the covariance matrix method to generate the random field for S_u as it is very simple and straightforward to implement. A single value of normalized horizontal scale fluctuation ($\theta_x/D = \theta_y/D$) is considered, and the normalized vertical scales of fluctuation (θ_z/D) are subjects of the parametric study. This paper presents the variations of probabilistic characteristics of the dimensionless bearing capacity factor (i.e., μ_{Nc} and CoV_{Nc}) for different m, CoV_{Su},

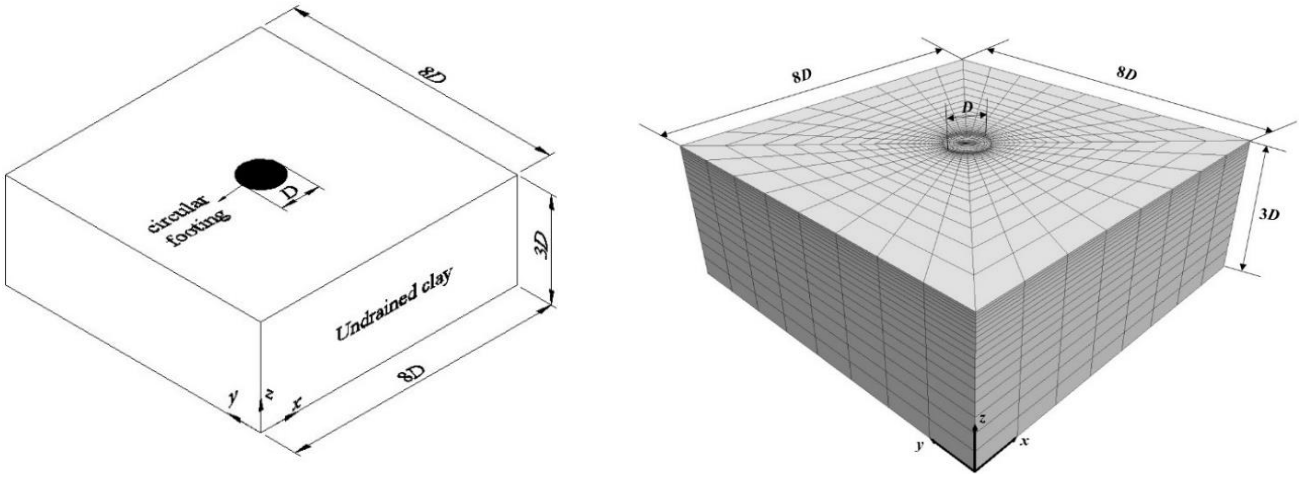

(a) (b)

Fig. 1 Circular footing on undrained clay: (a) schematic diagram and (b) finite-difference discretization

Table 2 Comparison of obtained N_c for circular footing with the available literature

	N_c				
m	Khatri and Kumar (2009)[a]	Houlsby and Martin (2003)[b]	Benmoussa *et al.* (2021)[c]	Kusakabe *et al.* (1986)[d]	Present study[e]
0	6.00	6.05	6.05	6.31	6.096
1	6.88	6.95	7.00	7.39	7.176
2	7.55	7.63	7.76	8.28	8.02
3	8.12	8.21	8.47	9.02	8.77

[a]Lower bound finite element limit analysis
[b]The method of stress characteristics
[c]Finite difference method (FLAC)
[d]Upper bound method
[e]Finite difference method (FLAC^{3D})

and θ_z/D. The successive section illustrates the variation of failure probability (p_f) for different factors of safety. In addition, the variations in the allowable design bearing capacity factor (N_{cd_all}) for different reliability indices (β), m, CoV_{Su}, and θ_z/D are also demonstrated in the present study.

2. Finite difference modeling

The schematic diagram of a three-dimensional surface circular footing (rough and rigid) resting on an undrained clay is shown in Fig. 1(a). The footing diameter (D) is considered as 2 m in this study. Three-dimensional finite-difference-based software, FLAC^{3D} (2012), is utilized to model the circular footing and the soil domain and perform all the numerical analyses. In the case of probabilistic analysis, the extent of the model domain in both horizontal directions is assumed to be 8D, and in the vertical direction, it is assumed to be 3D. The horizontal and the vertical displacements of the model are restricted at the bottom boundary, whereas the outer side boundaries are fixed in the lateral direction to allow only the vertical displacement. Since the S_u of the soil is considered non-random in the deterministic analysis, only a quarter of the symmetric domain is generated for this analysis, and the boundary conditions imposed are similar to the probabilistic analysis. Radially graded mesh around a cylindrical-shaped tunnel with solid fill is used to discretize the soil domain. The total number of elements is considered as 16128. The domain and mesh sizes of the soil model is chosen after several trials to maintain the balance between efficiency and accuracy. The domain and mesh convergence study of the model is carried out considering m = 0 (refer to Table 1). The relatively smaller size elements are chosen near the footing area (adjacent to the footing edge), where the high-stress gradient is expected. However, the mesh size gradually increases as it approaches the boundary. The discretized finite difference mesh is illustrated in Fig. 1(b). The clayey soil is assumed to follow the elastic-perfectly plastic Mohr-Coulomb yield criterion. In the deterministic analysis, the S_u of clay at the ground surface (i.e., S_{u0}) is considered as 25 kPa (Majumder and Chakraborty 2021). The elastic modulus (E) and the Poisson's ratio (v) are considered as 10 MPa and 0.45, respectively. The footing roughness is ensured by providing the lateral resistance at the nodes representing the footing area. An optimal and minimal amount of controlled downward velocity of magnitude 1×10^{-5} m/step is employed for the specified nodes. The footing bearing capacity is obtained by taking

Table 3 Comparison of deterministic bearing capacity of strip footing obtained from the present study with Li *et al.* (2015)

	S_u constant throughout the depth (kPa)	S_u linearly increasing with depth (kPa)
Li *et al.* (2015)	468	275
Present study	466.95	274.2

Table 4 Comparison of probabilistic bearing capacity of strip footing (for the non-stationary random field) obtained from the present study with Li *et al.* (2015).

	Normalized autocorrelation length	Number of Monte Carlo simulations	Mean bearing capacity (kPa)	Standard deviation of bearing capacity (kPa)
Li *et al.* (2015)	l_x/B = 2.5, l_z/B = 0.5, B = 2 m	500	272.2	18.2
Present study			271.73	18.74

the summation of the vertical reaction forces of the nodes defining the footing area and dividing it by the footing area. Then the model undergoes several steps until the ultimate value of bearing capacity is achieved (Halder and Chakraborty 2020a, Kawa and Pula 2020).

3. Validation of the present study

Since no probabilistic study is available for the circular footing considering the non-stationary random field for S_u, a comparison is made considering the deterministic results obtained from the present study with the existing literature (refer to Table 2) given as (a) the upper bound solution of N_c of rough circular footing considering the Prandtl type failure mechanism (Kusakabe *et al.* 1986), (b) the estimation of N_c of circular footing by Houlsby and Martin (2003) using the method of stress characteristics, (c) the lower bound calculation of N_c by Khatri and Kumar (2009) considering finite element method in association with linear programming, (d) the finite-difference solution of N_c by Benmoussa *et al.* (2021). It is evident from Table 2 that the present results are in between the lower bound and upper bound solutions of Khatri and Kumar (2009) and Kusakabe *et al.* (1986), respectively, and the obtained N_c values are comparatively higher than the finite difference solutions obtained by Benmoussa *et al.* (2021). This reason can be attributed to the three-dimensional model being considered for the present analysis, whereas the two-dimensional axisymmetric model was generated in their study. The present study is further compared with Li *et al.* (2015) by carrying out the probabilistic analysis of strip footing considering the non-stationary random field for S_u for a particular horizontal and vertical autocorrelation length. In their study, the increasing rate of S_u with depth (a) was considered as a random field, whereas the submerged unit weight (γ') of the soil was assumed to be a random variable. The mean values of a and γ' were assumed to be 1.4 and 11 kN/m^3, respectively. The S_u value at the ground surface was taken as 40 kPa. For the stationary case, the ultimate bearing capacity is calculated based on the S_u value at the mid-depth of the soil model. Hence, the bearing capacity for the stationary case was found to be higher than that for the non-stationary case. In the case of deterministic analysis, the comparison with the literature is made for both stationary and non-stationary cases (refer to Table 3). However, in the case of probabilistic analysis, the comparison is made only for the non-stationary case (refer to Table 4). The results obtained from the present study are in good agreement with the literature.

4. Probabilistic analysis

4.1 Generation of the spatially variable random field for S_u (non-stationary)

The spatially random characteristics of soil parameters (undrained shear strength, S_u for the present study) can be designated by mean (μ), standard deviation (σ) or the coefficient of variation (CoV), and autocorrelation length (l) or scale of fluctuation (θ) (Haldar and Sivakumar Babu 2008, Choudhuri and Chakraborty 2021). The lognormal distribution is chosen to simulate the random field for S_u (non-stationary) to avoid generating negative random numbers (Griffiths *et al.* 2002, Haldar and Sivakumar Babu 2008, Jha 2016). However, the elastic modulus (E) and Poisson's ratio (v) are considered to be non-random as the ultimate bearing capacity of the footing is almost irresponsive to these two parameters (Li *et al.* 2019). The mean value of S_{u0} is considered as 25 kPa, and the mean value of S_u at any arbitrary depth z where CoV_{Su} is constant can be expressed using the following equation

$$\mu_{Su} = \mu_{Su0} + \frac{mz\mu_{Su0}}{D} \tag{3}$$

where μ_{Su0} *and* μ_{Su} are the mean values of undrained shear strength at the ground surface and at a depth of z, respectively. Here, m = 0 represents the stationary random field, whereas m > 0 represents the non-stationary random fields.

A three-dimensional single exponential autocorrelation function, $\rho(\zeta)$, is assumed to generate the spatially varied non-stationary random field for S_u, given as follows (Kawa and Puła 2020)

Table 5 Summary of the probabilistic parameters used in the present study

Parameters	Values
Mean undrained shear strength at the ground surface, μ_{Su0} (kPa)	25
Coefficient of undrained shear strength, CoV_{Su} (%)	25, 50
Dimensionless strength gradient parameter, m	0, 1, 2, 3
Normalized horizontal scales of fluctuation ($\theta_x/D = \theta_y/D$)	5
Normalized vertical scale of fluctuation (θ_z/D)	0.5, 1, 2, 4

$$\rho(\xi_x,\xi_y,\xi_z) = \exp\left(\frac{-2|\xi_x|}{\theta_x} + \frac{-2|\xi_y|}{\theta_y} + \frac{-2|\xi_z|}{\theta_z}\right) \quad (4)$$

where $\xi_x = (x_i - x_j)$, $\xi_y = (y_i - y_j)$, and $\xi_z = (z_i - z_j)$ are the distances between the centroidal coordinates of the i^{th} and j^{th} elements (i = 1, 2, 3, …, and j = 1, 2, 3, …). Parameters θ_x, θ_y, and θ_z are the scales of fluctuation in the x, y, and z directions, respectively. The autocorrelation length (l) defines the length over which the random soil parameter values are strongly correlated to each other. Higher values of l define the smoothly varying random field, whereas lower values of l denote the ragged field (Griffiths *et al.* 2002). For the exponential autocorrelation function, $\theta = 2l$ (El-Ramly *et al.* 2003). In the present paper, the horizontal scales of fluctuation in both x and y directions are considered to be equal (i.e., $\theta_x = \theta_y$), following Kawa and Puła (2020). Because of the natural soil deposition process, the horizontal scales of fluctuation ($\theta_x = \theta_y$) are usually greater than the vertical scale of fluctuation (θ_z) (Jamshidi Chenari and Alaie 2015). Hence, the anisotropic random fields (i.e., $\theta_x = \theta_y \neq \theta_z$, more specifically $\theta_x = \theta_y > \theta_z$) are generated in the present study. The summary of the probabilistic parameters used in the present study is provided in Table 5.

The non-stationary random field of S_u is generated using the covariance matrix decomposition method (Haldar and Sivakumar Babu 2008, Kasama and Whittle 2016). After evaluating the autocorrelation matrix, $\rho(\xi)$, the matrix is decomposed into the lower triangular matrix (A) and its transpose (A^T) as follows

$$\rho(\chi) = AA^T \quad (5)$$

The autocorrelated standard normal non-stationary random field for S_u [$G(\ln \bar{S_u})$] is evaluated using the lower triangular matrix (A) given as follows

$$G(\ln \bar{S_u}) = \sum_{j=1}^{i} A_{ij} G_j(\ln S_u),\ i = 1, 2, 3, \ldots \quad (6)$$

where $G(\ln S_u)$ is the column vector of the uncorrelated standard normal variable having mean = 0 and variance = 1. Since the S_u of the clay is assumed to be lognormally distributed, the autocorrelated non-stationary random field can be evaluated as follows

$$S_u(\lambda) = \exp[\mu_{\ln S_u} + \sigma_{\ln S_u} G(\ln \bar{S_u})] \quad (7)$$

where $\lambda = \lambda(x, y, z)$ is the position in space where the random field of S_u is required. $\mu_{\ln S_u}$ and $\sigma_{\ln S_u}$ are evaluated using the following transformation

$$\sigma^2_{\ln S_u} = \ln(1 + COV^2_{Su}) \quad (8)$$

$$\mu_{\ln S_u} = \ln \mu_{Su} - \frac{1}{2}\sigma^2_{\ln S_u} \quad (9)$$

In FLAC^{3D}, the centroidal coordinates of all the elements of the finite difference mesh are extracted as a text file using the FISH subroutine and transferred to MATLAB (2020). The non-stationary random field for S_u is generated in MATLAB. The obtained field is again taken back to FLAC^{3D} in the form of the text file and allocated to each element using the FISH subroutine. The exemplary random fields of S_u for different m corresponding to a particular $\theta_x/D = \theta_y/D$, θ_z/D, and CoV_{Su} are illustrated in Fig. 2 (for three typical Monte Carlo realizations). Cross-sectional views of the random fields along the centroid of footing in the x-z plane are also shown in Fig. 2. The μ_{Nc} and CoV_{Nc} for each set of parameters given in Table 5 are evaluated using the Monte Carlo simulations technique. All the probabilistic analyses are run considering 500 simulations to achieve a better consistent result (refer to Fig. 3). It is to be mentioned that all the analyses (both deterministic and probabilistic) are done on a PC with 12 GB RAM and a single core of Intel Core i5 processor with a clock speed of 1.80 GHz, and it took around 33 hours of computational time to complete the 500 MC realizations of a particular set of probabilistic input statistics.

4.2 Failure probability

A footing is considered to fail under the ultimate limit state of collapse when the applied stress (q_{app}) on the footing is more than the ultimate bearing capacity (q_u) of the underlying soil. In the present study, the applied stress normalized by S_{u0} (i.e., q_{app}/S_{u0}) is considered to be the ultimate bearing capacity factor obtained from the deterministic analysis (i.e., N_{c_det}) (Griffiths *et al.* 2002, Haldar and Sivakumar Babu 2008, Halder and Chakraborty 2020a). Since the S_u of the clay is assumed to follow the lognormal distribution, the N_c values obtained from the probabilistic analysis are most likely to be lognormally distributed. However, it is verified by plotting the actual distribution of N_c with the hypothetical cumulative lognormal distribution having the parameters μ_{Nc} and CoV_{Nc} (refer to Fig. 4). The plotting is done for a particular case of

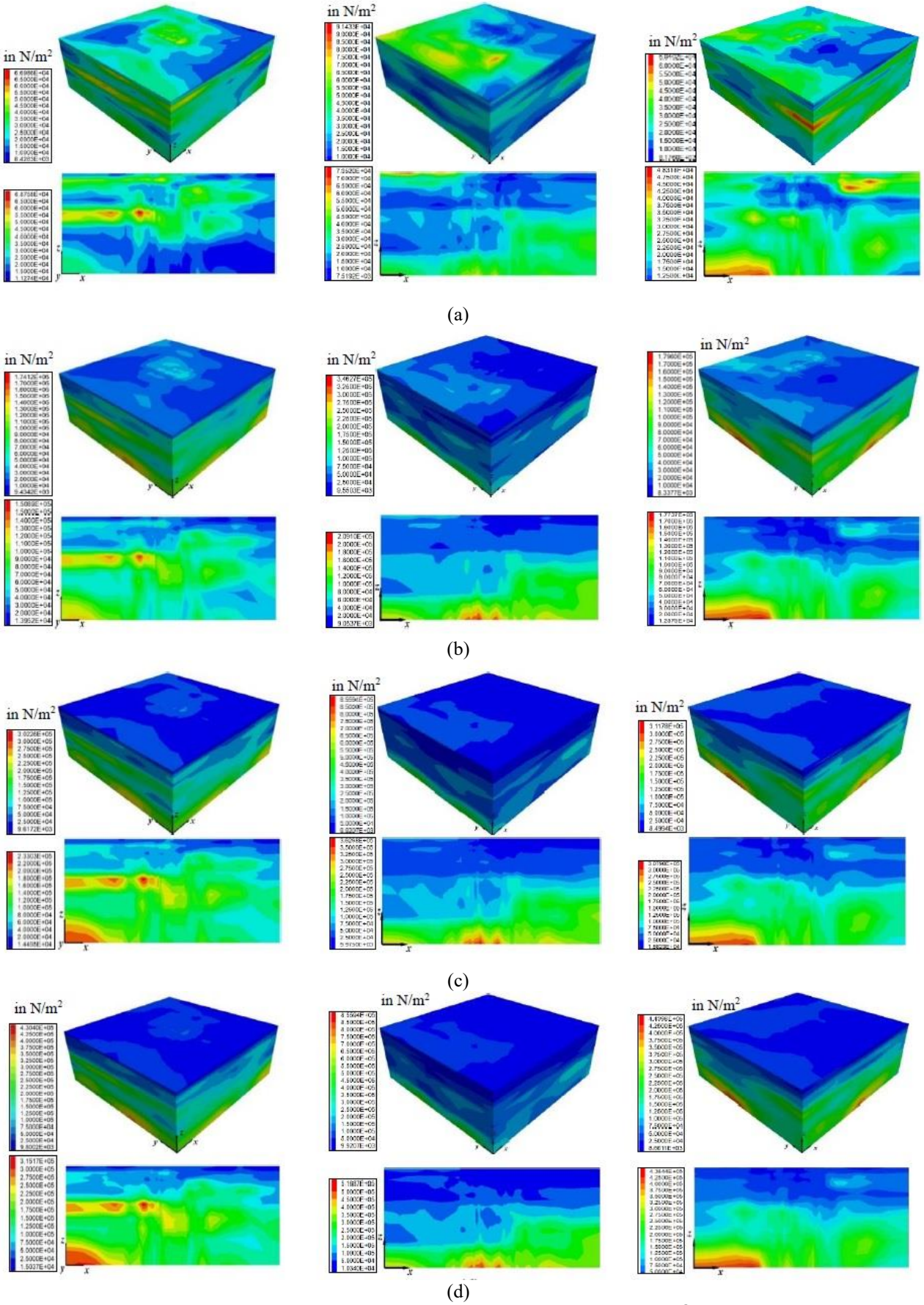

Fig. 2 The exemplary spatially varied random fields of undrained shear strength (in N/m^2) for three typical MC realizati ons considering (a) m = 0, (b) m = 1, (c) m = 2, and (d) m = 3 ($\theta_x/D = \theta_y/D$ = 5, θ_z/D = 0.5, CoV_{Su} = 50%)

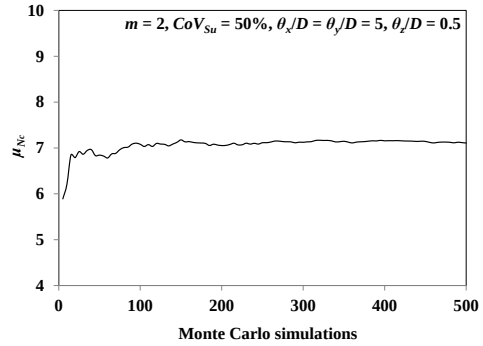

(a)

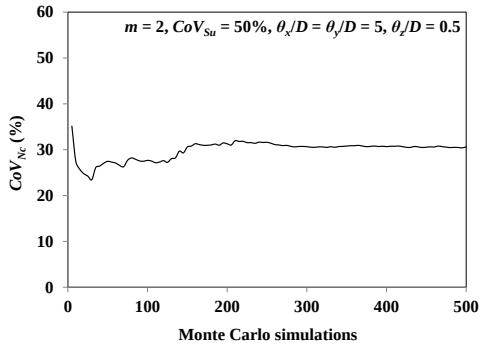

(b)

Fig. 3 Variations of (a) μ_{Nc} and (b) CoV_{Nc} for different Monte Carlo simulations corresponding to m = 2, CoV_{Su} = 50%, $\theta_x/D = \theta_y/D$ = 5, and θ_z/D = 0.5

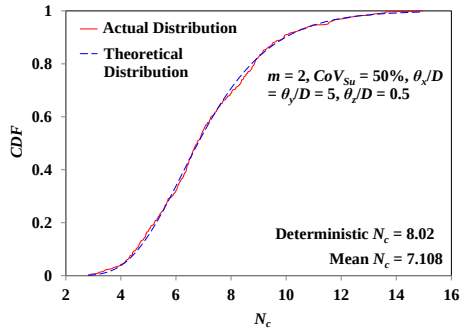

Fig. 4 Comparison between actual distribution and theoretical lognormal distribution of N_c for m = 2, CoV_{Su} = 50%, $\theta_x/D = \theta_y/D$ = 5, and θ_z/D = 0.5

m = 2, CoV_{Su} = 50%, $\theta_x/D = \theta_y/D$ = 5, and θ_z/D = 0.5. It is observed that the actual distribution agrees well with the hypothetical lognormal distribution. Thus, the failure probability (p_f) of the system can be defined as the probability for which the evaluated q_u normalized by S_{u0} (i.e., N_c) is less than the N_{c_det}, given as follows

$$p_f = P(q_u / S_{u0} < q_{app} / S_{u0}) = P(N_c < N_{c\_det}) = \Phi\left(\frac{\ln(N_{c\_det}) - \mu_{\ln N_c}}{\sigma_{\ln N_c}}\right) = \Phi(-\beta) \quad (10)$$

where $\Phi(.)$ denotes the cumulative normal distribution function. $\mu_{\ln N_c}$ and $\sigma_{\ln N_c}$ are the underlying normal distribution parameters, and β represents the reliability index.

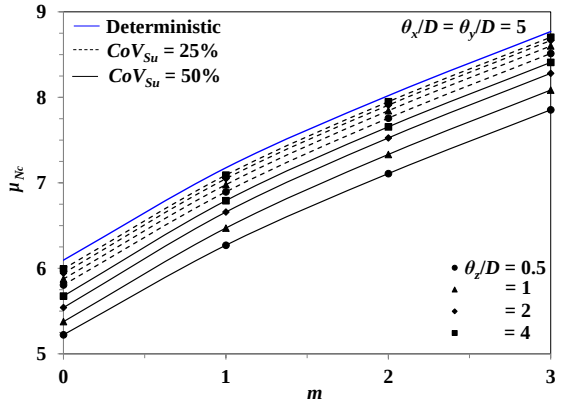

(a)

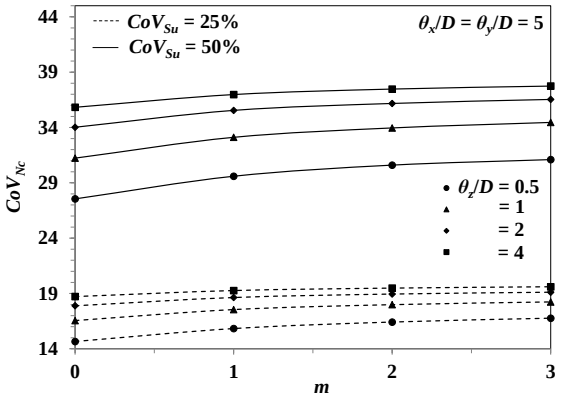

(b)

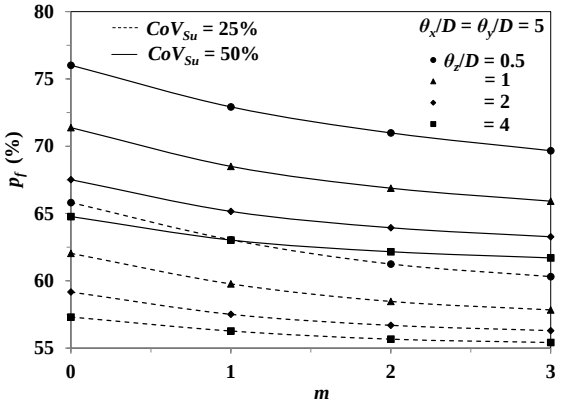

(c)

Fig. 5 Variations of (a) μ_{Nc}, (b) CoV_{Nc}, and (c) p_f with respect to different m, CoV_{Su}, and θ_z/D

5. Results obtained from the probabilistic analysis

The effects of m, CoV_{Su}, and θ_z/D on μ_{Nc}, CoV_{Nc}, and p_f are discussed in this section, followed by the details of the failure mechanism of the spatially varied soil under the footing. Then, the variations of cumulative and probability density functions (*CDF* and *PDF*) for different m, CoV_{Su}, and θ_z/D are discussed. In addition, the effect of the factor of safety (*FoS*) on p_f of the system for different CoV_{Su}, m, and θ_z/D is illustrated in this section. Finally, the allowable design N_c (N_{cd_all}) is evaluated for different β, and the variations of N_{cd_all} are also illustrated for different CoV_{Su}, m, and θ_z/D.

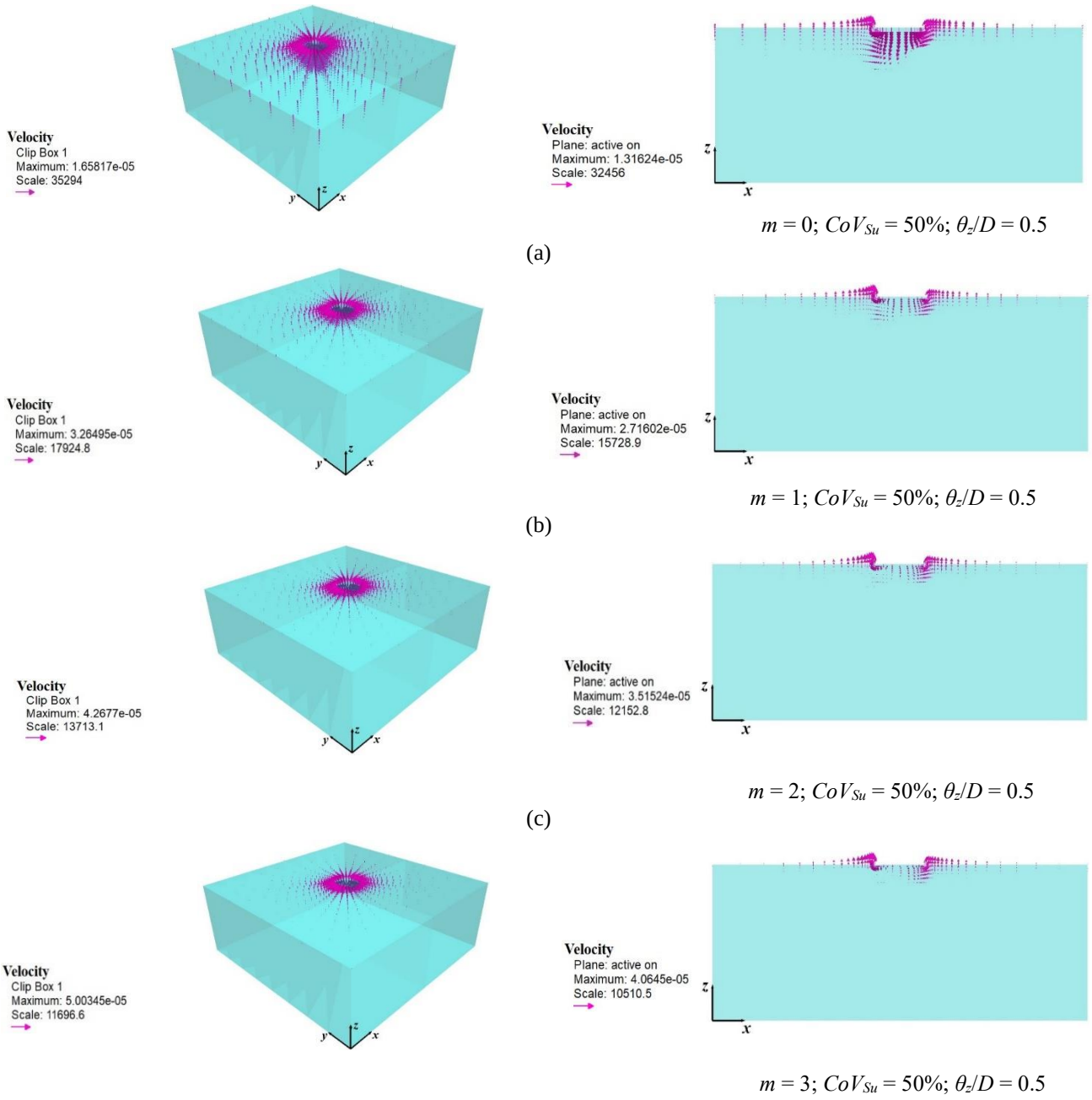

Fig. 6 The exemplary velocity vector plots for spatially variable undrained clay corresponding to (a) m = 0, (b) m = 1, (c) m = 2, and (d) m = 3 (CoV_{Su} = 50%, $\theta_x/D = \theta_y/D$ = 5, and θ_z/D = 0.5)

5.1 Variations of μ_{Nc}, CoV_{Nc}, and p_f for different m, CoV_{Su}, and θ_z/D

The effects of different m, CoV_{Su}, and θ_z/D on the μ_{Nc}, CoV_{Nc}, and p_f are illustrated in Figs. 5(a)-5(c), respectively.

***Effect of m*:** With the increase in dimensionless strength gradient parameter (m), both μ_{Nc} and CoV_{Nc} increase for the particular values of $\theta_x/D = \theta_y/D$, θ_z/D, and CoV_{Su}. The variation of μ_{Nc} follows a similar trend obtained for the deterministic analysis. However, the value of μ_{Nc} in each case is less than the deterministic bearing capacity factor (N_{c_det}). The increase in μ_{Nc} and CoV_{Nc} is non-linear with respect to m, concurring with the obtained trends for mean and CoV by Wu *et al.* (2020) in the case of surface strip footing, where the m value was also varied from 0 to 3. In contrast to μ_{Nc} and CoV_{Nc}, the p_f of the system decreases non-linearly as the m value increases.

***Effect of CoV_{Su}*:** With the increase in CoV_{Su}, the μ_{Nc} and CoV_{Nc} of the footing decreases and increases, respectively. The obtained trend is very intuitive as with the increase in CoV_{Su}, the randomness in S_u increases. Hence, the chances of producing weaker zones under the footing increase as the CoV_{Su} increases, leading to the failure of soil under the

footing due to the application of load. It is also found that the p_f of the system increases with the increase in CoV_{Su}.

Effect of θ_z/D: Both μ_{Nc} and CoV_{Nc} of the footing increase with the increase in θ_z/D. The reason behind an increase in CoV_{Nc} with θ_z/D can be attributed as for the lower values of θ_z/D, the generated field is very ragged, and the averaging effect is very prominent, leading to a significant variance reduction, whereas, for the higher values of θ_z/D, the generated field is smoothly varying. Because of that, the averaging effect is less prominent, and the variance reduction is less (Jha 2016). However, in contrast to μ_{Nc} and CoV_{Nc}, the p_f of the system decreases as the θ_z/D increases. The rate of increase in μ_{Nc} and CoV_{Nc} seizes as the θ_z/D increases. Similarly, the rate of change in p_f also decreases with the increase in θ_z/D. The obtained trend agrees well with Halder and Chakraborty (2020a) and Kawa and Pula (2020).

5.2 Failure patterns of the footing underlying soil

The paper presents the failure mechanisms for stationary and non-stationary random fields through the velocity vector plots. Fig. 6 shows such failure patterns for different dimensionless strength gradient parameters (i.e., m = 0, 1, 2,and 3) corresponding to a specific Monte Carlo realization, CoV_{Su}, and θ_z/D (i.e., CoV_{Su} = 50%, $\theta_x/D = \theta_y/D$ = 5, θ_z/D = 0.5). Cross-sectional views of the failure patterns along the centroid of footing in the x-z plane are also shown in Fig. 6 to visualize the failure mechanisms under the footing. The figure shows that the asymmetrical failure patterns are developed for the spatially variable soil irrespective of m. The depth of the plastic zones under the footing becomes shallower with the increase in m. The reason can be attributed to the increasing values of S_u of the soil along depth direction with the increase in m value. Thus, for higher m, the higher value of S_u will resist the soil shear path to go to the higher depth. Similar to the depth of plastic zones, the extent of the plastic zones beyond the edge of footing also reduces as the m value increases. A similar type of observation was reported by Kusakabe *et al.* (1986). It is also observed that the maximum magnitude of the velocity vector increases with the increase in m.

5.3 Variations of CDF and PDF for different m, CoV_{Su}, and θ_z/D

The variations of *CDF* and *PDF* for different m are illustrated in Fig. 7 for a particular CoV_{Su} and θ_z/D (i.e., CoV_{Su} = 50%, $\theta_x/D = \theta_y/D$ = 5, θ_z/D = 0.5). From the *CDF* plots, it can be stated that the cumulative probability (or the failure probability) decreases with the increase in m for a particular value of N_c. From the *PDF* plots, it can be observed that the maximum probability density decreases as the m value increases. For the lower values of N_c, the probability of occurrence decreases with the increase in m. In contrast, for the higher values of N_c, the probability of occurrence increases with the increase in m. In their study for strip footing, Shen *et al.* (2020) reported that the effect of the gradient of undrained shear strength (k) was very

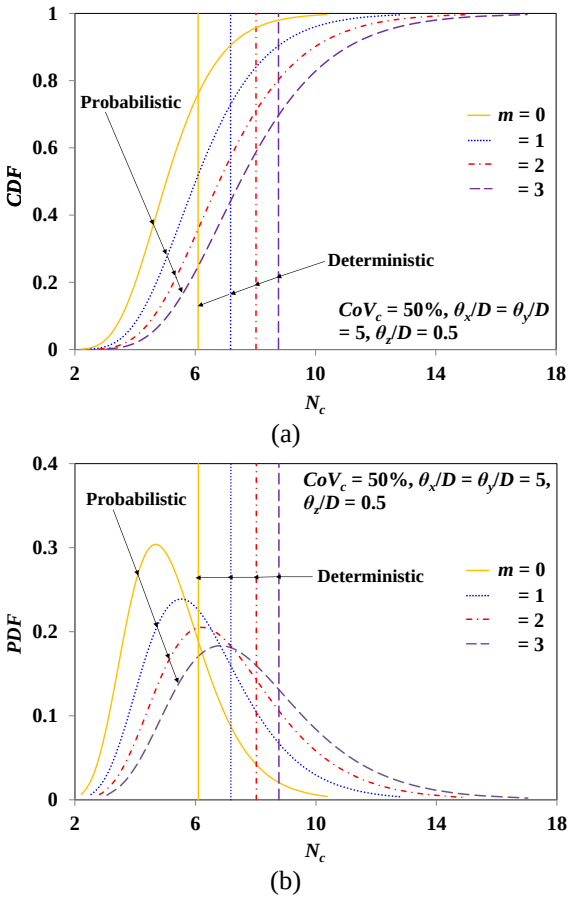

Fig. 7 Variations of (a) *CDF* and (b) *PDF* with respect to different m for CoV_{Su} = 50%, $\theta_x/D = \theta_y/D$ = 5, and θ_z/D = 0.5

minimal for the lower bearing capacity values as the portion of *CDF* and *PDF* plots were falling in a very tight band. However, for the higher values of the bearing capacity factor, the presently obtained trend concurs with the observed trend by Shen *et al.* (2020).

Fig. 8 illustrates the variations of *CDF* and *PDF* for two different values of CoV_{Su} corresponding to a particular value of m and θ_z/D (i.e., m = 2, $\theta_x/D = \theta_y/D$ = 5, θ_z/D = 0.5). It is observed from the *CDF* plot that the p_f increases with the increase in CoV_{Su} for the lower values of N_c. At the deterministic bearing capacity factor (N_{c_det}), the failure probability is also higher for the higher value of CoV_{Su}. However, the failure probability reduces with the increase in CoV_{Su} for the higher values of N_c. It can be observed from the *PDF* plot that the N_c value at the maximum probability of occurrence is less than the N_{c_det}, and it reduces with the increase in CoV_{Su}, which implies that the higher values of CoV_{Su} cause a significant reduction in N_c as compared to N_{c_det}. It is also observed that the maximum probability of occurrence decreases with the increase in CoV_{Su}, and the *PDF* curve becomes more asymmetric as the CoV_{Su} increases.

The variations of *CDF* and *PDF* for different θ_z/D are shown in Fig. 9 for the constant values of m and CoV_{Su} (i.e., m = 2, CoV_{Su} = 50%, $\theta_x/D = \theta_y/D$ = 5). For the lower values of N_c, the cumulative probability increases as the θ_z/D

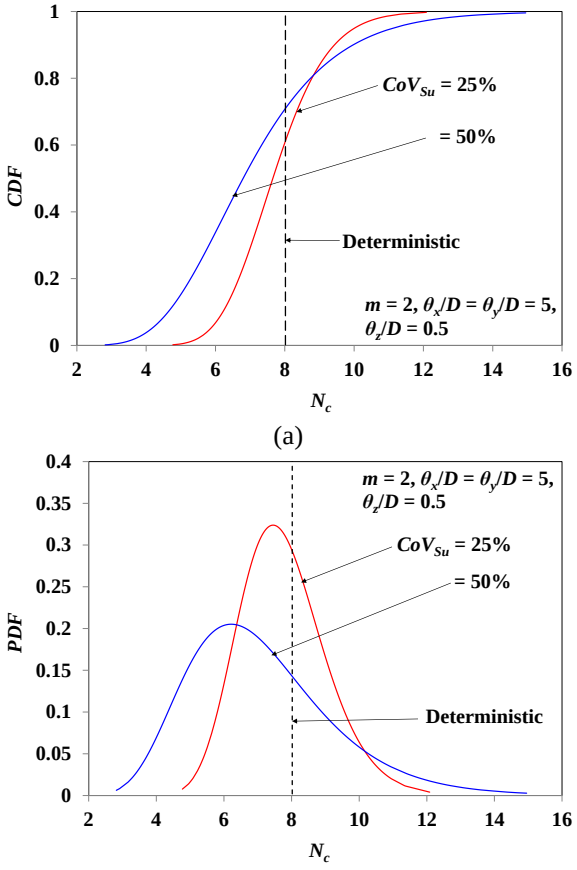

Fig. 8 Variations of (a) *CDF* and (b) *PDF* for different CoV_{Su} corresponding to m = 2, $\theta_x/D = \theta_y/D$ = 5, and θ_z/D = 0.5

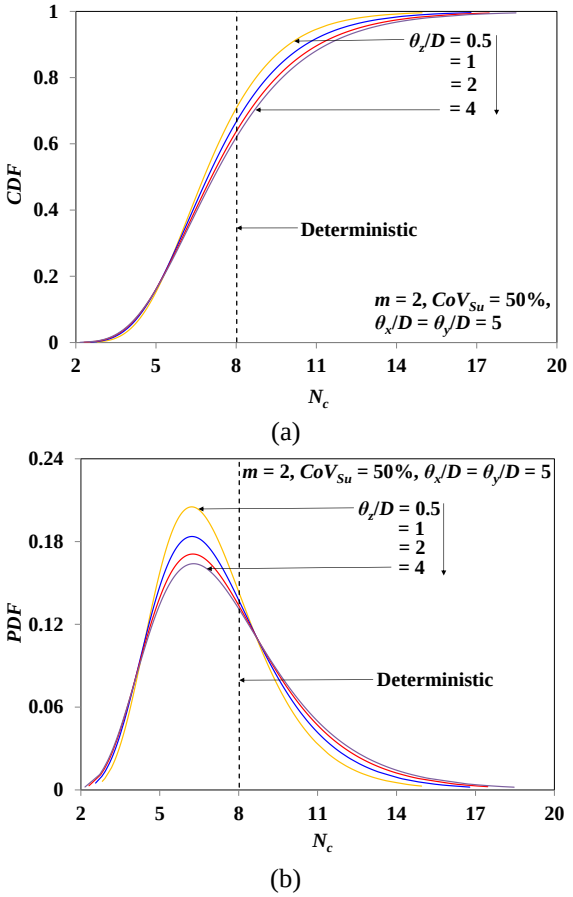

Fig. 9 Variations of (a) *CDF* and (b) *PDF* for different θ_z/D corresponding to m = 2, CoV_{Su} = 50%, and $\theta_x/D = \theta_y/D$ = 5

increases. Although, they are falling into a tight band. However, the cumulative probability decreases at the deterministic bearing capacity factor as the θ_z/D increases. Similar observations can also be made at the higher values of N_c. It can be clearly stated from the *PDF* plot that the maximum probability density decreases as the θ_z/D increases, and the probability of occurrence increases with the increase in θ_z/D for the higher values of N_c. It is also observed that the area under the *PDF* curve for θ_z/D = 0.5 lies more toward the left side of the N_{c_det} as compared to the θ_z/D = 4. It implies that the number of N_c values on the left of the N_{c_det} is more for θ_z/D = 0.5 than θ_z/D = 4. Thus, the failure probability (p_f) is higher for θ_z/D = 0.5 than that for θ_z/D = 4. The observation is similar to what has been obtained from the *CDF* plot.

5.4 Variations of p_f vs. FoS for different m, CoV_{Su}, and θ_z/D

The traditional factor of safety (*FoS*) concept has been used over the past years to account for the uncertainty associated with the material properties. However, incorporating the factor of safety into a structure does not ensure that the structure is completely safe against failure. It signifies the importance of conducting the probabilistic analysis, which ultimately helps in calculating the failure probability (p_f). A strong relationship exists between the p_f and the *FoS*. Thus, the failure probability accounting for the *FoS* can be calculated by modifying Eq. (10) as follows

$$p_f = P(N_c < N_{c\_\det} / FoS) = \Phi\left(\frac{\ln(N_{c\_\det}/FoS) - \mu_{\ln N_c}}{\sigma_{\ln N_c}}\right) = \Phi(-\beta) \quad (11)$$

The variations of failure probability (p_f) for different *FoS* and CoV_{Su} corresponding to m = 2, $\theta_x/D = \theta_y/D$ = 5, θ_z/D = 0.5 are illustrated in Fig. 10(a). It is clear from the figure that the p_f decreases drastically with the increase in the factor of safety. Though, the observation is very intuitive. In the case of CoV_{Su} = 25%, the failure probability becomes close to zero at *FoS* = 2, whereas the failure probability is about 4.42% for CoV_{Su} = 50%. Moreover, in the case of CoV_{Su} = 50%, the system is not entirely safe even at *FoS* = 3, as the failure probability is found to be 0.12%. Hence, using the conventional *FoS* concept may lead to overestimating the footing bearing capacity for the lower values of CoV_{Su} and underestimating the bearing capacity in the case of higher values of CoV_{Su} (Krishnan and Chakraborty 2022).

The variations of failure probability (p_f) with respect to *FoS* for different m ($\theta_x/D = \theta_y/D$ = 5, θ_z/D = 0.5, and CoV_{Su} = 50%) are illustrated in Fig. 10(b). The p_f of the system is

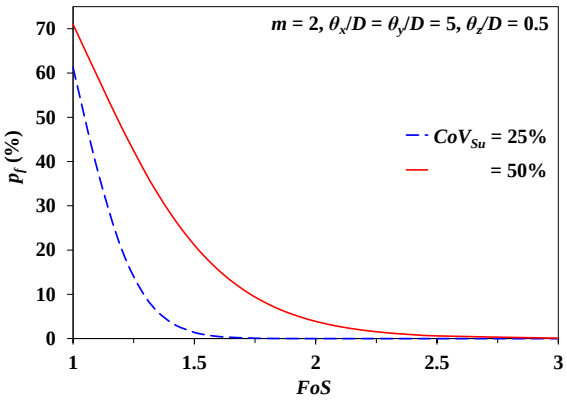

(a)

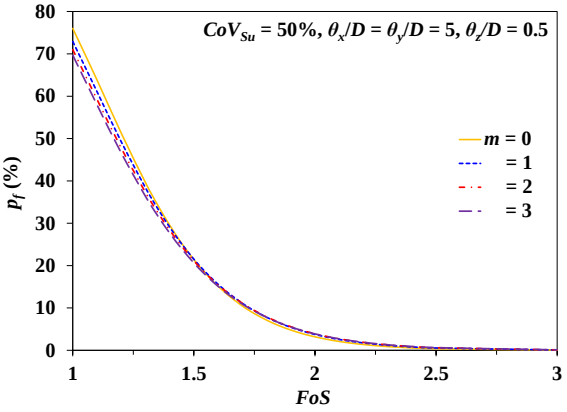

(b)

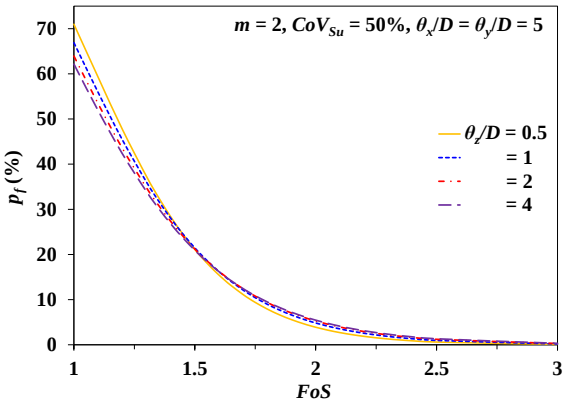

(c)

Fig. 10 Variations of p_f for different values of (a) CoV_{Su}, (b) m, and (c) θ_z/D

found to be maximum for m = 0 and minimum for m = 3 when FoS = 1, whereas the trend is observed to be opposite when the FoS varies from 2 to 3. However, the differences in failure probability are found to be very insignificant when $FoS \geq 1.5$. Similarly, the variations of p_f with respect to FoS for different θ_z/D (m = 2; $\theta_x/D = \theta_y/D$ = 5, and CoV_{Su} = 50%) are illustrated in Fig. 10(c). For FoS = 1, the p_f of the system decreases with the increase in θ_z/D (as discussed in subsection 5.1). However, for the higher values of FoS (i.e., $FoS \geq 1.563$), the p_f of the system starts increasing with the increase in θ_z/D. Griffiths and Fenton (2004) and Halder and Chakraborty (2020a) also reported a similar trend in their studies.

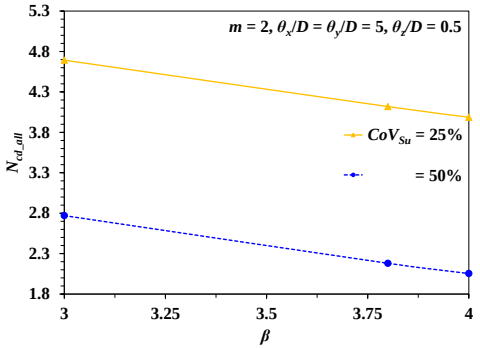

(a)

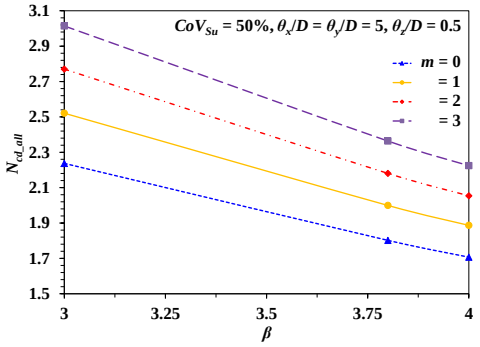

(b)

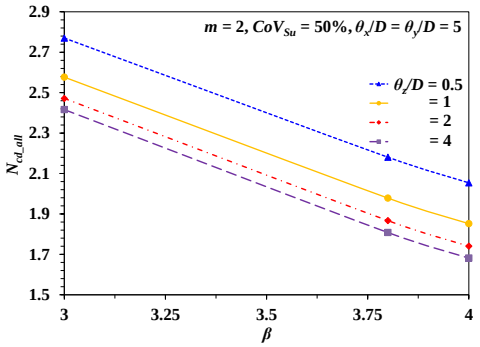

(c)

Fig. 11 Variations of N_{cd_all} with respect to reliability indices (β) for different values of (a) CoV_{Su}, (b) m, and (c) θ_z/D

5.5 Variations of allowable design N_c for different β, CoV_{Su}, m, and θ_z/D

Based on the observations perceived in the previous subsection (i.e., subsection 5.4), the allowable design bearing capacity factor (i.e., N_{cd_all}) can be evaluated using the following equation

$$\Phi\left(\frac{\ln(N_{cd\_all}) - \mu_{\ln N_c}}{\sigma_{\ln N_c}}\right) = \Phi(-\beta) \tag{12}$$

$$N_{cd\_all} = \exp(\mu_{\ln N_c} - \beta\sigma_{\ln N_c}) \tag{13}$$

Three different reliability indices are utilized in the study to evaluate the allowable design N_c of the footing: (a) β = 3.8 which corresponds to the RC2 reliability class structures (residential and office buildings and their typical foundations) having medium consequences of failure, and

50 years of design working life (EN1990 2002); (b) β = 3.0 for the average performance, and (c) β = 4.0 for the good performance of the geotechnical structures provided by USACE (1997). The variations of N_{cd_all} with respect to β (residential and office buildings and their typical foundations) having medium consequences of failure, and 50 years of design working life (EN1990 2002); (b) β = 3.0 for the average performance, and (c) β = 4.0 for the good performance of the geotechnical structures provided by USACE (1997). The variations of N_{cd_all} with respect to β.

6. Conclusions

The present paper explores the effect of Case III non-stationary random field on the probabilistic characteristics of the bearing capacity of a circular footing resting on the surface of a clayey soil under vertical loading. The soil properties adopted in this study are from the available literature. The m, CoV_{Su}, and θ_z/D are the subjects of the parametric study. The present study also depicts the variations of p_f for different FoS corresponding to the different values of CoV_{Su}, m, and θ_z/D. The major conclusive remarks obtained from the study are given as follows:

• CoV_{Nc} and p_f of the system increases and decreases, respectively, non-linearly with the increase in dimensionless strength gradient parameter (m). The effect of CoV_{Su} is very prominent as the increase in CoV_{Su} causes a significant decrease and increase in the mean bearing capacity factor (μ_{Nc}) and the failure probability (p_f), respectively. Both μ_{Nc} and CoV_{Nc} increase as the θ_z/D increases, whereas p_f reduces as the θ_z/D increases.

• The maximum probability density decreases as the m value increases. For the lower values of N_c, the probability of occurrence decreases with the increase in m, whereas it increases with m for the higher values of N_c. In the case of the CDF plot, the cumulative probability decreases with the increase in m value for a particular N_c.

• The system is found to be not entirely safe for the higher values of safety factors as it has a non-zero value of failure probability. The factor of safety concept overestimates the bearing capacity of the footing for the lower values of CoV_{Su}, whereas it underestimates the bearing capacity for the higher CoV_{Su} values. For FoS = 1, the p_f of the system decreases with the increase in θ_z/D, and it increases for the higher values of FoS. For the variations to different m, the p_f of the system is almost irresponsive to m for $FoS \geq 1.5$.

• The allowable design bearing capacity factor (N_{cd_all}) decreases with an increase in reliability index (β). Similarly, for the specific value of β and m, the N_{cd_all} decreases with the increase in CoV_{Su} and θ_z/D. However, the N_{cd_all} increases with the increase in m for the particular values of β, CoV_{Su}, and θ_z/D.

The present study provides a primary perception of a problem based on the three-dimensional probabilistic analysis of circular footing on spatially varied clay, considering S_u increasing with depth subjected to vertical loading and the results are presented in a non-dimensional form. The variations in the failure probability of the system are also studied for different parameters. In general, offshore shallow foundations are constructed on marine clay deposits, where S_u of the clay linearly increases with depth (Bransby and Randolph 1998, Shen *et al.* 2020). Hence, it is expected that the results and charts provided in the study will be helpful for the engineers dealing with the offshore shallow foundations located on the marine clay deposit.

References

Al-Bittar, T. and Soubra, A. -H. (2013), "Bearing capacity of strip footings on spatially random soils using sparse polynomial chaos expansion", *Int. J. Numer. Anal. Methods Geomech*., **37**(13), 2039-2060. https://doi.org/10.1002/nag.2120.

Bai, T., Yang, H., Chen, X., Zhang, S. and Jin, Y. (2020), "In-situ monitoring and reliability analysis of an embankment slope with soil variability", *Geomech. Eng.*, **23**(3), 261-273. https://doi.org/10.12989/gae.2020.23.3.261.

Benmoussa, S., Benmebarek, S. and Benmebarek, N. (2021), "Bearing capacity factor of circular footings on two-layered clay soils", *Civ. Eng. J.*, **7**(5), 775-785. https://doi.org/10.28991/cej-2021-03091689.

Bishop, A.W. (1966), "The strength of soils as engineering materials", *Géotechnique*, **16**(2), 91-130. https://doi.org/10.1680/geot.1966.16.2.91.

Bransby, M.F. and Randolph, M.F. (1998), "Combined loading of skirted foundations", *Géotechnique*, **48**(5), 637-655. https://doi.org/10.1680/geot.1998.48.5.637.

Charlton, T.S. and Rouainia, M. (2017), "A probabilistic approach to the ultimate capacity of skirted foundations in spatially variable clay", *Struct. Saf.*, **65**, 126-136. https://doi.org/10.1016/j.strusafe.2016.05.002.

Cho, S.E. (2010), "Probabilistic assessment of slope stability that considers the spatial variability of soil properties", *J. Geotech. Geoenviron. Eng.*, **136**(7), 975-984. https://doi.org/10.1061/(ASCE)GT.1943-5606.0000309.

Choudhuri, K. and Chakraborty, D. (2021), "Probabilistic Bearing Capacity of a Pavement Resting on Fibre Reinforced Embankment Considering Soil Spatial Variability", *Front. Built Environ.*, **7**, 628016. https://doi.org/10.3389/fbuil.2021.628016.

Choudhuri, K. and Chakraborty, D. (2022), "Probabilistic analyses of three-dimensional circular footing resting on two-layer c–ϕ soil system considering soil spatial variability", *Acta Geotech.*, **17**(12), 5739-5758. https://doi.org/10.1007/s11440-022-01701-7.

Choudhuri, K. and Chakraborty, D. (2023) "Risk assessment of three-dimensional bearing capacity of a circular footing resting on spatially variable sandy soil", *Iran. J. Sci. Technol. - Trans. Civ. Eng.*, **47**(6), 3681-3698. https://doi.org/10.1007/s40996-023-01129-3.

Choudhuri, K. and Chakraborty, D. (2024), "Probability-based analyses of bearing capacity of square and rectangular footings resting on sandy soil considering rotational anisotropy", *Acta Geotech.*, 1-22. https://doi.org/10.1007/s11440-024-02297-w.

Chwała, M. and Kawa, M. (2021), "Random failure mechanism method for assessment of working platform bearing capacity with a linear trend in undrained shear strength", *J. Rock Mech. Geotech. Eng.*, **13**(6), 1513-1530. https://doi.org/10.1016/j.jrmge.2021.06.004.

Das, S. and Chakraborty, D. (2024), "Influence of rotated anisotropy and spatial variability of undrained clay on bearing capacity of strip footings under eccentric loading", *Comput. Geotech.*, **172**, 106443. https://doi.org/10.1016/j.compgeo.2024.106443.

Deng, Z.P., Pan, M., Niu, J.T., Jiang, S.H. and Qian, W.W. (2021), "Slope reliability analysis in spatially variable soils using sliced inverse regression-based multivariate adaptive regression spline", *Bull. Eng. Geol. Environ.*, **80**, 7213-7226. https://doi.org/10.1007/s10064-021-02353-9.

Deng, Z.P., Pan, M., Niu, J.T. and Jiang, S.H. (2022), "Full probability design of soil slopes considering both stratigraphic uncertainty and spatial variability of soil properties", *Bull. Eng. Geol. Environ.*, **81**(5), 195. https://doi.org/10.1007/s10064-022-02702-2.

El-Ramly, H., Morgenstern, N.R. and Cruden, D.M. (2003), "Probabilistic stability analysis of a tailings dyke on presheared clay-shale", *Can. Geotech. J.*, **40**(1), 192-208. https://doi.org/10.1139/t02-095.

EN1990 (2002), Basis of structural design, European Committee for Standardization; Brussels, Belgium.

Fenton, G.A. and Griffiths, D.V. (2002), "Probabilistic foundation settlement on spatially random soil", *J. Geotech. Geoenviron. Eng.*, **128**(5), 381-390. https://doi.org/10.1061/(ASCE)1090-0241(2002)128:5(381).

FLAC^{3D} (2012), Fast Lagrangian analysis of continua, version 5.01: user's and theory manuals, Itasca Consulting Group Inc., Minneapolis, USA.

Griffiths, D.V., Fenton, G.A. and Manoharan, N. (2002), "Bearing capacity of rough rigid strip footing on cohesive soil: probabilistic study", *J. Geotech. Geoenviron. Eng.*, **128**(9), 743-755. https://doi.org/10.1061/(ASCE)1090-0241(2002)128:9(743).

Griffiths, D.V. and Fenton, G.A. (2004), "Probabilistic slope stability analysis by finite elements", *J. Geotech. Geoenviron. Eng.*, **130**(5), 507-518. https://doi.org/10.1061/(ASCE)1090-0241(2004)130:5(507).

Griffiths, D.V. and Fenton, G.A. (2009), "Probabilistic settlement analysis by stochastic and random finite-element methods", *J. Geotech. Geoenviron. Eng.*, **135**(11), 1629-1637. https://doi.org/10.1061/(ASCE)GT.1943-5606.0000126.

Haldar, S. and Sivakumar Babu, G.L. (2008), "Effect of soil spatial variability on the response of laterally loaded pile in undrained clay", *Comput. Geotech.*, **35**, 537-547. https://doi.org/10.1016/j.compgeo.2007.10.004.

Halder, K. and Chakraborty, D. (2020a), "Influence of soil spatial variability on the response of strip footing on geocell-reinforced slope", *Comput. Geotech.*, **122**, 103533. https://doi.org/10.1016/j.compgeo.2020.103533.

Halder, K. and Chakraborty, D. (2020b) "Probabilistic bearing capacity of strip footing on reinforced anisotropic soil slope", *Geomech. Eng.*, **23**(1), 15-30 https://doi.org/10.12989/gae.2020.23.1.015.

Houlsby, G.T. and Martin, C.M. (2003), "Undrained bearing capacity factors for conical footings on clay", *Géotechnique*, **53**(5), 513-520. https://doi.org/10.1680/geot.2003.53.5.513.

Jamshidi Chenari, R. and Mahigir, A. (2014), "The effect of spatial variability and anisotropy of soils on bearing capacity of shallow foundations", *Civ. Eng. Infrastruct. J.*, **47**(2), 199-213. https://doi.org/10.7508/ceij.2014.02.004.

Jamshidi Chenari, R. and Alaie, R. (2015), "Effects of anisotropy in correlation structure on the stability of an undrained clay slope", *Georisk*, **9**(2), 109-123. https://doi.org/10.1080/17499518.2015.1037844.

Jha, S.K. (2016), "Reliability-based analysis of bearing capacity of strip footings considering anisotropic correlation of spatially varying undrained shear strength", *Int. J. Geomech.*, **16**(5), 06016003. https://doi.org/10.1061/(ASCE)GM.1943-5622.0000638.

Jiang, S.H. and Huang, J. (2018), "Modeling of non-stationary random field of undrained shear strength of soil for slope reliability analysis", *Soils Found.*, **58**(1), 185-198. https://doi.org/10.1016/j.sandf.2017.11.006.

Jiang, S.H., Huang, J., Griffiths, D.V. and Deng, Z.P. (2022), "Advances in reliability and risk analyses of slopes in spatially variable soils: A state-of-the-art review". *Comput. Geotech.*, **141**, 104498. https://doi.org/10.1016/j.compgeo.2021.104498.

Kasama, K. and Whittle, A.J. (2016), "Effect of spatial variability on the slope stability using Random Field Numerical Limit analysis", *Georisk*, **10**(1), 42-54. https://doi.org/10.1080/17499518.2015.1077973.

Kawa, M. and Puła, W. (2020), "3D bearing capacity probabilistic analyses of footings on spatially variable *c-ϕ* soil", *Acta Geotech.*, **15**(6), 1453-1466. https://doi.org/10.1007/s11440-019-00853-3.

Khatri, V.N. and Kumar, J. (2009), "Bearing capacity factor Nc under $\phi = 0$ condition for piles in clays", *Int. J. Numer. Anal. Methods Geomech.*, **33**(9), 1203-1225. https://doi.org/10.1002/nag.763.

Krishnan, K. and Chakraborty, D. (2022), "Probabilistic study on the bearing capacity of strip footing subjected to combined effect of inclined and eccentric loads", *Comput. Geotech.*, 141, 104505,. https://doi.org/10.1016/j.compgeo.2021.104505.

Kusakabe, O., Suzuki, H. and Nakase, A. (1986), "An upper bound calculation on bearing capacity of a circular footing on a non-homogeneous clay", *Soils Found.*, **26**(3), 143-148. https://doi.org/10.3208/sandf1972.26.3_143.

Li, D.Q., Qi, X.H., Phoon, K.K., Zhang, L.M. and Zhou, C.B. (2014), "Effect of spatially variable shear strength parameters with linearly increasing mean trend on reliability of infinite slopes", *Struct. Saf.*, **49**, 45-55. https://doi.org/10.1016/j.strusafe.2013.08.005.

Li, D.Q., Qi, X.H., Cao, Z.J., Tang, X.S., Zhou, W., Phoon, K.K. and Zhou, C.B. (2015), "Reliability analysis of strip footing considering spatially variable undrained shear strength that linearly increases with depth", *Soils Found.*, **55**(4), 866-880. https://doi.org/10.1016/j.sandf.2015.06.017.

Li, Y., Liu, K., Zhang, B. and Xu, N. (2019), "Reliability of shape factors for bearing capacity of square footings on spatially varying cohesive soils", *Int. J. Geomech.*, **20**(3), 04019195. https://doi.org/10.1061/(ASCE)GM.1943-5622.0001614.

Li, T., Gong, W. and Tang, H. (2021), "Three-dimensional stochastic geological modeling for probabilistic stability analysis of a circular tunnel face", *Tunn. Undergr. Sp. Tech.*, **118**, 104190. https://doi.org/10.1016/j.tust.2021.104190.

Li, T., Pan, Q., Shen, Z. and Gong, W. (2022), "Probabilistic stability analysis of a tunnel face in spatially random Hoek–Brown rock masses with a multi-tangent method", *Rock Mech. Rock Eng.*, **55**(6), 3545-3561. https://doi.org/10.1007/s00603-022-02821-y.

Lombardi, M., Cardarilli, M. and Raspa, G. (2017), "Spatial variability analysis of soil strength to slope stability assessment", *Geomech. Eng.*, **12**(3), 483-503. https://doi.org/10.12989/gae.2017.12.3.483.

Luo, Z., Atamturktur, S., Cai, Y. and Juang, C.H. (2011), "Reliability analysis of basal- heave in a braced excavation in a 2-D random field", *Comput. Geotech.*, **39**, 27-37. https://doi.org/10.1016/j.compgeo.2011.08.005.

Lumb, P. (1966), "The variability of natural soils", *Can. Geotech. J.*, **3**(2), 74-97. https://doi.org/10.1139/t66-009.

Majumder, M. and Chakraborty, D. (2021), "Three-dimensional numerical analysis of under-reamed pile in clay under lateral loading", *Innov. Infrastruct. Solut.*, **6**(2), 1-17. https://doi.org/10.1007/s41062-020-00428-2.

Sivakumar Babu, G.L. and Mukesh, M.D. (2004), "Effect of soil variability on reliability of soil slopes", *Géotechnique*, **54**(5), 335-337. https://doi.org/10.1680/geot.2004.54.5.335.

Shen, Z., Jin, D., Pan, Q., Yang, H. and Chian, S.C. (2020),

"Probabilistic analysis of strip footings on spatially variable soils with linearly increasing shear strength", *Comput. Geotech.*, **126**, 103653. https://doi.org/10.1016/j.compgeo.2020.103653.

Shen, Z., Jin, D., Pan, Q., Yang, H. and Chian, S.C. (2021), "Effect of soil spatial variability on failure mechanisms and undrained capacities of strip foundations under uniaxial loading", *Comput. Geotech.*, **139**, 104387. https://doi.org/10.1016/j.compgeo.2021.104387.

Shu, S., Gao, Y. and Wu, Y. (2020), "Probabilistic bearing capacity analysis of spudcan foundation in soil with linearly increasing mean undrained shear strength", *Ocean Eng.*, **204**, 106800. https://doi.org/10.1016/j.oceaneng.2019.106800.

Srivastava, A. and Sivakumar Babu, G.L. (2009), "Effect of soil variability on the bearing capacity of clay and in slope stability problems", *Eng. Geol.*, **108**(1-2), 142-152. https://doi.org/10.1016/j.enggeo.2009.06.023.

Srivastava, A. and Sivakumar Babu, G.L. (2011), "Deflection and buckling of buried flexible pipe-soil system in a spatially variable soil profile", *Geomech. Eng.*, **3**(3), 169-188. https://doi.org/10.12989/gae.2011.3.3.169.

The MathWorks Inc. (2020), MATLAB (R2020b), version 9.9, Massachusetts, United States. https://www.mathworks.com

U.S. Army Corps of Engineers (USACE) (1997), Engineering and design: Introduction to probability and reliability methods for use in geotechnical engineering, Eng. Circ. 1110-2-547, U.S. Dept. of the Army, Washington, DC.

Wu, Y., Zhou, X., Gao, Y., Zhang, L. and Yang, J. (2019), "Effect of soil variability on bearing capacity accounting for non-stationary characteristics of undrained shear strength", *Comput. Geotech.*, **110**, 199-210. https://doi.org/10.1016/j.compgeo.2019.02.003.

Wu, Y., Zhou, X., Gao, Y. and Shu, S. (2020), "Bearing capacity of embedded shallow foundations in spatially random soils with linearly increasing mean undrained shear strength", *Comput. Geotech.*, **122**, 103508. https://doi.org/10.1016/j.compgeo.2020.103508.

Yi, J.T., Huang, L.Y., Li, D.Q. and Liu, Y. (2020), "A large-deformation random finite-element study: failure mechanism and bearing capacity of spudcan in a spatially varying clayey seabed", *Géotechnique*, **70**(5), 392-405. https://doi.org/10.1680/jgeot.18.P.171.

Yoo, C. (2016), "Effect of spatial characteristics of a weak zone on tunnel deformation behavior", *Geomech. Eng.*, **11**(1), 41-58. https://doi.org/10.12989/gae.2016.11.1.041.

Zhao, C., Gong, W., Li, T., Juang, C.H., Tang, H. and Wang, H. (2021), "Probabilistic characterization of subsurface stratigraphic configuration with modified random field approach", *Eng. Geol.*, **288**, 106138. https://doi.org/10.1016/j.enggeo.2021.106138.

Zhu, D., Griffiths, D.V., Huang, J. and Fenton, G.A. (2017), "Probabilistic stability analyses of undrained slopes with linearly increasing mean strength", *Géotechnique*, **67**(8), 733-746. https://doi.org/10.1680/jgeot.16.P.223.

CC